New good ionic conductor: Ba-deficient Ba$_3$Y$_4$O$_9$ with Zr substitution

Katsuhiro Ueno[*], Naoyuki Hatada[*], and Tetsuya Uda[*]

Department of Materials Science and Engineering, Kyoto University,

Yoshida Honmachi, Sakyo-ku, Kyoto, 606-8501, Japan

* Corresponding authors: Katsuhiro Ueno (ueno.katsuhiro.87s@st.kyoto-u.ac.jp),

Naoyuki Hatada (hatada.naoyuki.8u@kyoto-u.ac.jp),

and Tetsuya Uda (uda_lab@aqua.mtl.kyoto-u.ac.jp)

Tel: +81-75-753-5445, Fax: +81-75-753-5284

Declarations

Conflicts of interest

There are no conflicts to declare.

Availability of data and material

The datasets generated during and/or analyzed during the current study are available from the

corresponding authors on reasonable requests.

Keywords

fuel cells, SOFC, electrolyzer, oxygen ion conductor, $Ba_3Y_4O_9$

Abstract

To lower operating temperatures of solid oxide fuel cells (SOFCs), the development of ion-conducting

oxides with high conductivity and durability is desired. In this work, we investigated Zr-substituted

"$Ba_3Y_4O_9$" as an ionic conductor at intermediate temperatures and found that the Zr substitution for Y

dramatically improves the phase stability in humidified atmospheres at 300-800 °C. The total electrical

conductivity of 20 mol% Zr-substituted $Ba_3Y_4O_9$ is about 1 mS/cm at 700 °C in dry H_2 and O_2

atmospheres and the contribution of electronic conduction (both hole and electron) is relatively small

compared with Y-doped $BaZrO_3$ (BZY) and Gd-doped CeO_2 (GDC) which are typical intermediate-

temperature ionic conductors. Besides, in the Zr-substituted "$Ba_3Y_4O_9$" samples, we observed that

BaO-rich amorphous phase coexists with the main phase whose composition is estimated to be

Ba:(Y+Zr) ~ 2:3. Therefore, the main conducting phase might be Ba-deficient $Ba_3Y_4O_9$. The

mechanism of the ionic conduction and the improvement of chemical stability has not been revealed

yet due to the lack of crystallographic information about the Ba-deficient phase. While we are now

working on further investigation, we promptly report the characteristic of the new compound.

1   Introduction

Ionic conducting oxides at intermediate temperatures (400-700 °C) are under active development to

lower the operating temperatures of solid oxide fuel cells (SOFCs) and extend choices for structural

materials[1,2]. The promising candidates include oxide-ion conductors such as Gd-doped CeO_2 (GDC)[3,4]

and $La_{0.9}Sr_{0.1}Ga_{0.8}Mg_{0.2}O_{3-\delta}$ (LSGM)[5,6] and proton conductors such as Y-doped $BaZrO_3$ (BZY) and

$BaCeO_3$ (BCY)[7–10], but they have some problems in terms of chemical stabilities or electron/hole

conductions[10–13]. The electron/hole conductions in reducing/oxidizing atmospheres result in the

occurrence of the internal current leakage in electrolytes in SOFCs and reduce the energy efficiency[14,15].

Therefore, the further development of pure ionic conductors at intermediate temperatures is still

important for the realization of intermediate-temperature solid oxide fuel cells (IT-SOFCs) with high

efficiency and durability.

Recently, we found that the zirconium (Zr) can substitute for yttrium (Y) in $Ba_3Y_4O_9$ up to 47 mol%

at 1600 °C[16], promising the generation of some defects which may influence the conductivity behavior.

According to literature, $Ba_3Y_4O_9$ has a hexagonal perovskite-related structure with lattice parameters

$a = 6.114$ Å, $c = 25.21$ Å[17,18], and has been mainly investigated as phosphor candidates and nitric

monoxide (NO) direct decomposition catalysts with the substitution of trivalent cations or transition

metal ion for Y^{3+} [19–26]. Although other hexagonal perovskite-related oxides containing barium such as

$Ba_7Nb_4MoO_{20}$[27] and $Ba_5Er_2Al_2ZrO_{13}$[28] are expected as good ionic conductors, $Ba_3Y_4O_9$ has received

little attention as an ionic conductor probably because of the chemical instability to water and carbon

dioxide as well as the non-existence of oxygen vacancy in a unit cell[17,29,30].

In this work, we investigated the influence of Zr substitution for $Ba_3Y_4O_9$ in chemical stability to water

and conductivity behavior in dry H_2, dry O_2, and wet O_2 atmospheres at the intermediate temperatures

by heat-temperature X-ray diffraction (HT-XRD) analysis and A. C. impedance spectroscopy,

respectively. Besides, phase compositions and formation of secondary phases in the Zr-substituted

$Ba_3Y_4O_9$ samples are analyzed by an electron probe microanalyzer (EPMA).

2 Experimental

2.1 Material preparation

B3Y4-Z0, 10, 20 samples with nominal compositions $Ba_3(Y_{4-x}Zr_x)O_{9+0.5x}$ (x = 0, 0.4, 0.8) were

prepared by conventional solid state reaction method as described below. $BaCO_3$ (Wako Pure Chemical

Industries, Ltd., Japan, 99.9 %), Y_2O_3 (Shin-Etsu Chemical Co., Ltd., Japan, 99.9 %), and ZrO_2 (Tosoh

Corporation, Japan, 97.031 %) powders were used as raw materials and mixed at the desired ratios.

The mixtures were put into polyvinyl bottles with 2-propanol and yttria-stabilized zirconia (YSZ) balls

and were ball-milled for 24 hours. Then, the YSZ balls were removed by a stainless steel sieve, and

then 2-propanol was removed by vacuum drying. The sample powder was calcined at 1000 °C for 10

hours in ambient air and ball-milled for 24 hours again. After being pressed into disk-shaped pellets of

19 mm in diameter under 9.8 MPa, the samples were calcined at 1300 °C for 10 hours in ambient air.

The samples were pulverized with a zirconia mortar, ball-milled for 100 hours. The samples were

pressed into pellets under 420 MPa and sintered at 1600 °C for 24 hours in a dry Ar-20 % O_2

atmosphere. To suppress BaO evaporation during the sintering[31], the pellets were embedded in

sacrificial powder which had the same composition as the samples and calcined at 1300 °C.

6

2.2 Characterization

Phases were identified by powder X-ray diffraction (XRD) analysis with an X'Pert-ProMPD with

Cu$K\alpha$ radiation (PANalytical, Netherland). Microstructure observation and compositional analysis

were performed by an electron probe microanalyzer (EPMA) equipped with a wavelength dispersive

X-ray spectrometer (WDS) with a JXA-8530F (JEOL, Japan). The apparent density of the pellet-like

samples was measured by the Archimedes method and the relative density to the theoretical density

of $Ba_3Y_4O_9$[17] was calculated.

The chemical stabilities in humidified O_2 were tested by high-temperature powder XRD analysis

with the same XRD device using an HTK 1200N high-temperature chamber (Anton Paar, Graz,

Austria). The water vapor pressure was kept at ~0.02 atm by bubbling O_2 gas through deionized

water kept at room temperature. The samples were heated or cooled to the desired temperatures at a

rate of 20 °C/min.

The electrical conductivities of the B3Y4-Z10 and B3Y4-Z20 samples with sputtered platinum (Pt)

electrodes were measured in dry O_2, dry H_2, and humidified O_2 atmospheres. The water vapor

pressure was kept at ~0.02 atm by the same technique for HT-XRD measurement. After kept at 720

°C for 10 hours in dry O_2/H_2 atmospheres and 20 hours in humidified O_2, the samples were cooled

down at a rate of 0.2 °C/min with collecting A. C. impedance spectra in the frequency range from 10

Hz to 7 MHz using a frequency response analyzer (Solartron SI 1260, Solartron Analytical, UK) with

an applied voltage of 100 mV under open-circuit condition.

3   Results

3.1   Composition range of "$Ba_3Y_4O_9$"

Fig. 1 shows the powder XRD patterns of the samples after sintering. Although there are minor peaks

attributed to Y_2O_3, most of the diffraction peaks belong to $Ba_3Y_4O_9$. The peak positions change with

the increase in the Zr content, indicating the change of lattice parameter due to the substitution of Zr^{4+}

for Y^{3+}. The peak shift behaviors of B3Y4-Z10 and B3Y4-Z20 samples are similar to those confirmed

in our previous paper[16]. As shown in the results of the WDS point analysis in Fig. 2, the chemical

compositions of the $Ba_3Y_4O_9$-structured main phases in the B3Y4-Z10 and B3Y4-Z20 samples are

$Ba:(Y+Zr) \sim 2:3$, differing from the expected ratio of $Ba:(Y+Zr) = 3:4$. Therefore the main phase might

be better described as "Ba-deficient $Ba_3Y_4O_9$" rather than "$Ba_3Y_4O_9$" in terms of chemical composition.

Besides, the coexistence of BaO-rich phases with the main phases is confirmed in all samples. ‡ From

the results of XRD, the BaO-rich phases are probably amorphous, indicating the formation of liquid

phases during the sintering.⸸ It is noted that the sacrifice powder stuck to the pellet of the B3Y4-Z0

sample after sintering, reinforcing the hypothesis. Therefore, $Ba_3Y_4O_9$ is not a single-phase

composition but a mixture of two or more phases. However, in accordance with the reported literature,

we still call the mixture "$Ba_3Y_4O_9$" in this report until completing more detailed investigations.

‡ Footnote: From the WDS spectra, the existence of SiO_2 was confirmed in the BaO-rich phases and the concentration was about 5 mass%. Because the average concentrations of SiO_2 in the samples after heat-treatment at 1300 °C were about 1 mass%, the contamination of SiO_2 might occur in the synthesis process with Al_2O_3 crucible (0.1 wt% SiO_2). Now we are working on the sample preparation without SiO_2 contamination.

¶ Footnote: From the microstructure observation as shown in Fig. S1 in supplemental information, the morphology of the B3Y4-Z0 sample also suggests the existence of the liquid phase.
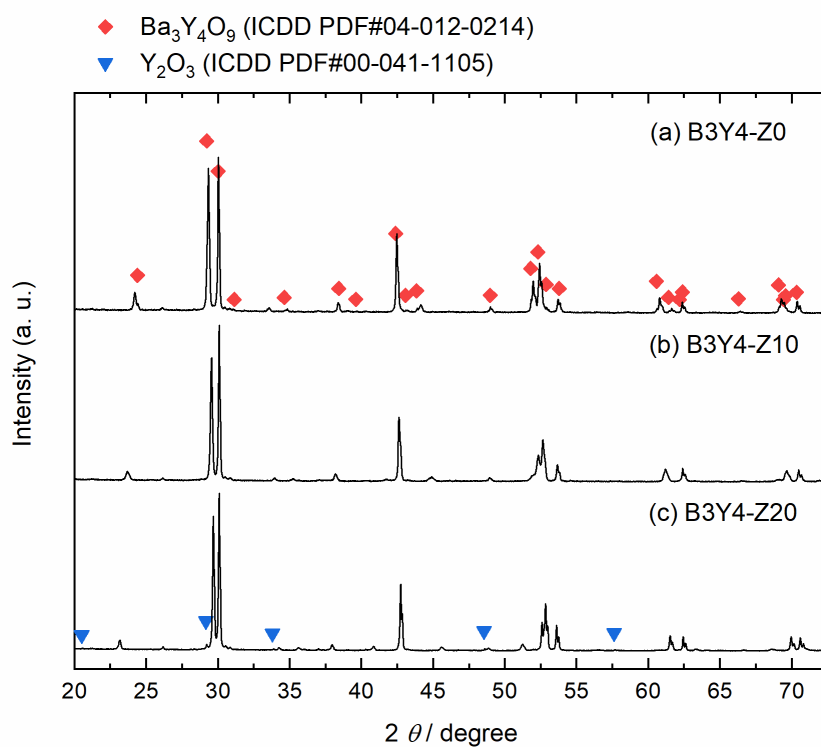
Fig. 1 The powder XRD patterns of (a) B3Y4-Z0, (b) B3Y4-Z10, and (c) B3Y4-Z20 samples at room temperature in an ambient atmosphere. All samples were sintered at 1600 °C for 24 hours in dry Ar-20 % O_2.
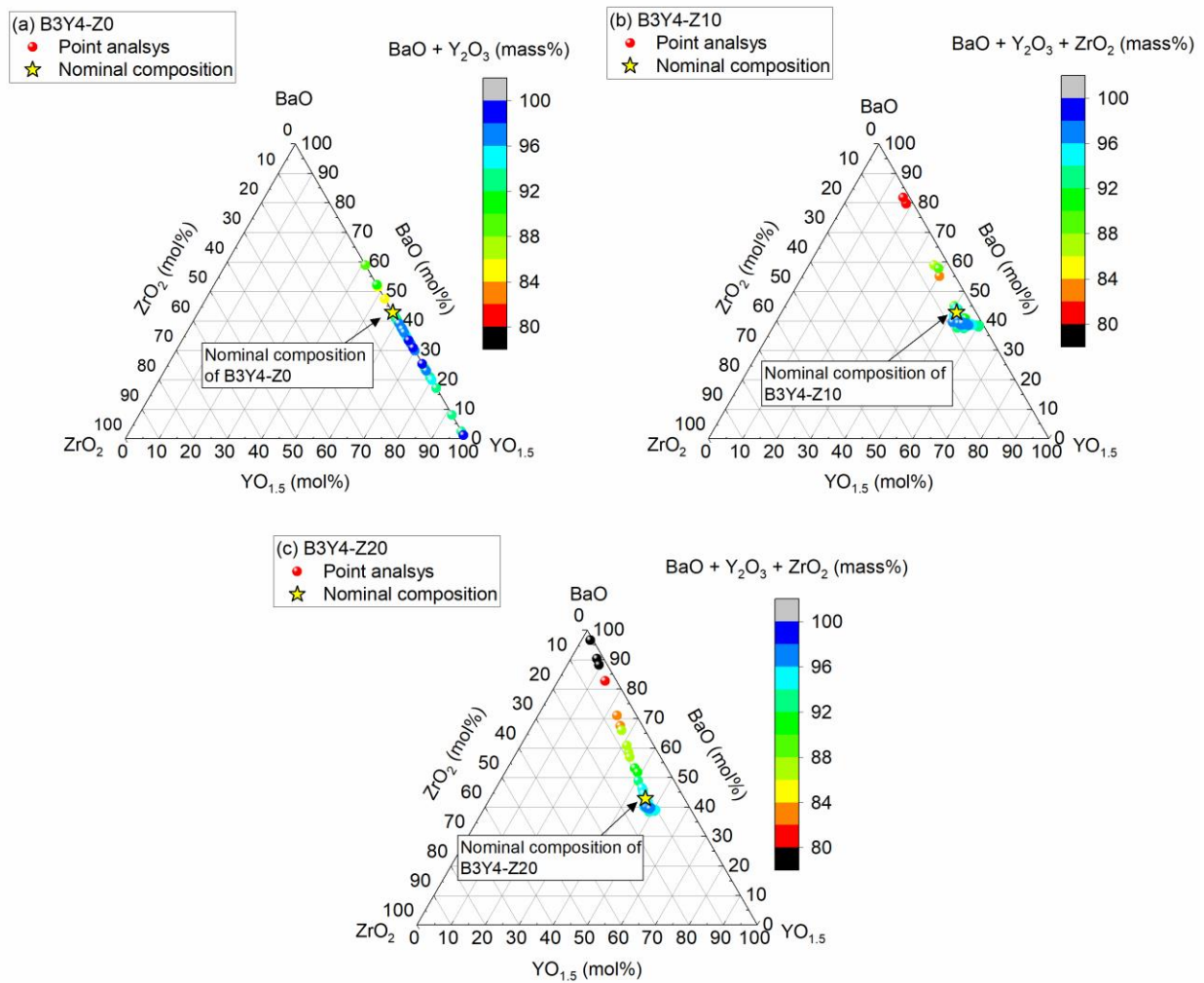
Fig. 2 Compositions of the polished cross-section of (a) B3Y4-Z0, (b) B3Y4-Z10, and (c) B3Y4-Z20 pellets as analyzed by EPMA-WDS. All samples were sintered at 1600 °C for 24 hours in dry Ar-20 % O_2. It is noted that the existence of SiO_2 in the BaO-rich phase was confirmed from the WDS spectra.

3.2 Chemical stability in humidified atmospheres

The results of high-temperature powder XRD analysis for the B3Y4-Z(0, 10, 20) samples are shown

in Fig. 3, indicating that the chemical stability of the $Ba_3Y_4O_9$–structured main phase in a humidified

atmosphere is dramatically improved by the substitution of Zr for Y. As shown in Fig. 3 (a), in

humidified atmospheres, $Ba_3Y_4O_9$ without the Zr substitution decompose to $Ba(OH)_2$ and Y_2O_3 at 300

°C during heating and then the diffraction peaks attributed to $Ba(OH)_2$ disappear at 400-500 °C. It

suggests the melting of $Ba(OH)_2$ phase, being in good agreement with the melting point of $Ba(OH)_2$

(~400 °C) in the previous report[32]. After the heat-treatment up to 800 °C in a humidified atmosphere,

several decomposed phases are confirmed in the B3Y4-Z0 sample. On the other hand, as shown in Fig.

3 (b) and (c), the crystallized "$Ba_3Y_4O_9$" phase still remained through the heat-treatment in humidified

atmospheres in the B3Y4-Z10 and B3Y4-Z20 samples. These results suggest that the substitution of

Zr for Y prevents the $Ba_3Y_4O_9$-structured main phase from decomposition. Interestingly, there is less

change in the diffraction pattern of the 20 % substituted sample than 10 %, indicating that the chemical

stability of Zr-substituted $Ba_3Y_4O_9$–structured main phase in a humidified atmosphere enhances with

the Zr content.
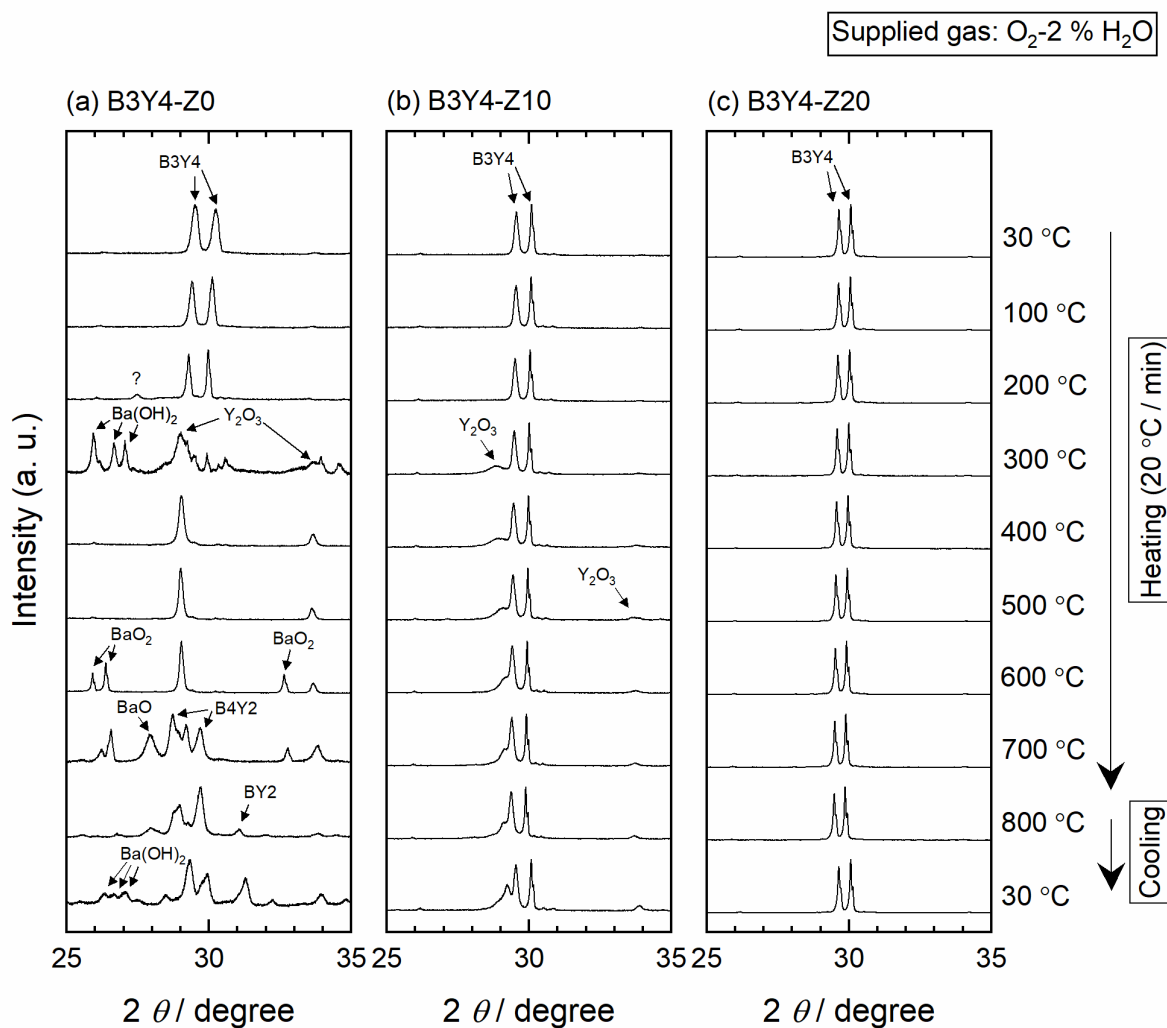
Fig. 3 High-temperature powder XRD patterns of (a) B3Y4-Z0, (b) B3Y4-Z10, and (c) B3Y4-Z20 samples in humidified O_2 atmospheres. The heating/cooling rate is 20 °C/min and the partial water pressure in humidified O_2 gas is kept at ~0.02 atm by bubbling in deionized water kept at room temperature. The phase identification from diffraction peaks was performed by comparing them with reference patterns in the ICDD database (BaO (PDF#01-071-3780), Y_2O_3 (PDF#00-041-1105), Ba(OH)$_2$ (PDF#00-044-0585), BaO_2 (PDF#03-065-6619), $Ba_3Y_4O_9$ (PDF#04-012-0214), $Ba_4Y_2O_7$ (PDF#00-037-0992), and BaY_2O_4 (PDF#01-082-2319)). B3Y4, B4Y2, and BY2 in this figure indicate the compounds $Ba_3Y_4O_9$, $Ba_4Y_2O_7$, and BaY_2O_4, respectively.

3.3 Conductivity behavior in dry/humidified atmospheres

The conductivities of the B3Y4-Z10 and B3Y4-Z20 samples in various atmospheres are compared in Fig. 4. For the B3Y4-Z10 sample, the conductivities in dry H_2 and humidified O_2 atmospheres have local maximum values at around 400 °C whereas that in dry O_2 atmosphere decreases with a decrease in temperature monotonically as shown in Fig. 4 (a). In contrast, for the B3Y4-Z20 sample, the conductivities in any atmospheres monotonically decrease with a decrease in temperature as shown in Fig. 4 (b). The conductivities of the B3Y4-Z20 sample derive from the $Ba_3Y_4O_9$-structured main phase because the decomposition is not confirmed in the B3Y4-Z20 sample from the HT-XRD measurement (Fig. 3 (c)). Thus the increase in the conductivities of the B3Y4-Z10 sample in 400-500 °C in dry H_2 and humidified O_2 atmospheres probably derives from the decomposed amorphous phase detected in the WDS analysis. Although dry H_2 gas contains water hardly, water may be generated from the reduction of oxide layers on materials in the measurement equipment.

The little difference in the conductivity of the B3Y4-Z20 sample in dry H_2/dry O_2/humidified O_2 atmospheres suggests that the dominant conducting species are oxide ions[†]. Over 500 °C, the conductivity of the B3Y4-Z20 sample in a dry O_2 atmosphere is slightly higher than that in a dry H_2

atmosphere, indicating the occurrence of the hole conduction. The transport number of hole ($t_{h^\bullet}$) is

estimated by (σ (in dry O_2) − σ (in dry H_2)) / σ (in dry O_2)) and is 0.23 at 700 °C, 0.21 at 600 °C, and

0.08 at 500 °C. The total conductivity of the sample in the dry H_2 atmosphere is about 1 mS/cm at

~700 °C, indicating that Ba-deficient $Ba_3Y_4O_9$ with Zr substitution is a good ionic conductor at

intermediate temperatures.

† Footnote: Because the conductivity in a humidified O_2 atmosphere was measured after the

measurement in a dry O_2 atmosphere, the difference in conductivities between dry and humidified O_2

atmospheres probably corresponding to time degradation.
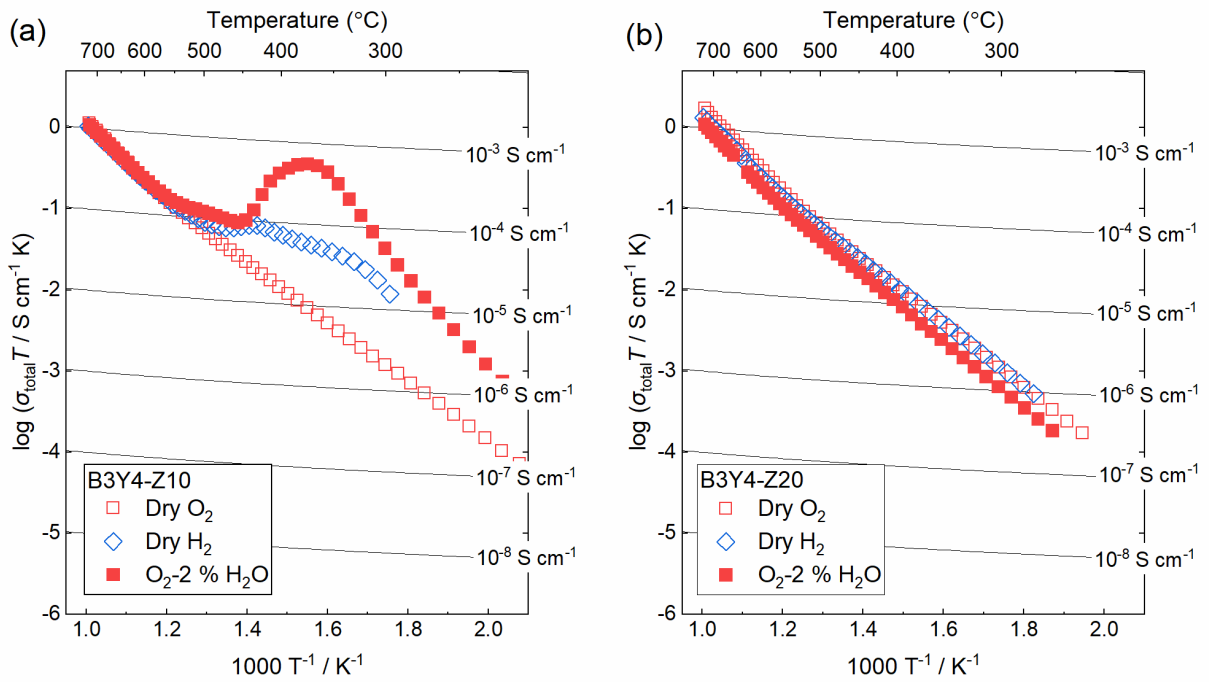
Fig. 4 Arrhenius plots of total conductivities of (a) the B3Y4-Z10 and (b) B3Y4-Z20 samples in various atmospheres. All samples were sintered at 1600 °C for 24 hours in dry Ar-20 % O_2. The conductivities were evaluated from A. C. impedance spectra collected with a 100 mV applied voltage under open-circuit condition. The samples were cooled down at a rate of 0.2 °C/min and the partial water pressure in humidified O_2 is kept at ~0.02 atm by bubbling in deionized water kept at room temperature.

4　Discussion

In terms of the chemical stability to water and the relatively high conductivity with a low contribution of holes, Ba-deficient $Ba_3Y_4O_9$ with Zr substitution is a good ionic conductor at the intermediate temperatures. For the application of electrolytes in IT-SOFCs, the chemical stability to water is required due to exposure to humidified atmospheres. Because $Ba_3Y_4O_9$ is considered as an unpromising candidate for an ionic conductor due to the chemical instability to water[17,29], the improvement of the chemical stability by Zr substitution for Y is an interesting finding in this work.

Besides, the ionic conductivity of the B3Y4-Z20 sample is remarkable and its total conductivity of 1 mS/cm at 700 °C is comparative to protonic conductors for IT-SOFCs such as Sr-doped LaP_3O_9[33], $La_{6.63}W_{1.17}O_{13.43}$[34], and $La_2(Nb_{0.3}Y_{0.7})_2O_{7-\delta}$[35]. In addition, the transport number of holes at the temperature in an oxidizing atmosphere is 0.23, which is much smaller than typical ionic conductors such as BZY (the transport number of hole is 0.77 in an oxidizing atmosphere)[11] and GDC (the transport number of electron is ~1 in a reducing atmosphere)[4]. Therefore, although more improvement in the conductivity is needed, Ba-deficient $Ba_3Y_4O_9$ has promising characteristics for the application of electrolytes in IT-SOFCs.

In the meanwhile, for understanding the mechanism of how Zr substitution in Ba-deficient $Ba_3Y_4O_9$

affects the chemical stability to water and ionic conduction, there is a strong need to reveal the actual

crystal structure of Ba-deficient $Ba_3Y_4O_9$. Recently, Fang *et al.* reported that co-doping of scandium

and cupper into $Ba_3Y_4O_9$ improves phase stability under NO, O_2, and H_2O co-existence condition and

proposed that smaller ionic size of Sc^{3+} (VI) (0.730 Å) than Y^{3+} (VI) (0.892 Å) may stabilize the crystal

structure geometrically[19]. However, we need to determine the crystallographic structure and

composition. It allows the first principle calculation and reveals the conduction mechanism in the

atomic scale. We are now working on further investigation.

5   Conclusions

In this work, the influence of Zr substitution for Y in "$Ba_3Y_4O_9$" on the chemical stability and the conductivity behavior were investigated. From EPMA-WDS analysis, we observed that BaO-rich amorphous phase coexists with the main phase with the chemical composition of Ba:(Y+Zr) ~ 4:6 in the Zr-substituted $Ba_3Y_4O_9$ samples, indicating that $Ba_3Y_4O_9$ is not a single-phase composition but a mixture of two or more phases. The main phase might be better described as Ba-deficient $Ba_3Y_4O_9$ in terms of chemical compositions. The chemical stability to water vapor at intermediate temperature (300-800 °C) improves by the increase in Zr content in the compounds and the decomposition of the crystallized main phase does not occur in the "20 % Zr-substituted $Ba_3Y_4O_9$" sample. Besides, the total conductivity of the "20 % Zr-substituted $Ba_3Y_4O_9$" sample is about 1 mS/cm in dry H_2/O_2 at 700 °C and the contributions of electron/hole conduction (transport number of holes ~ 0.23 at 700 °C in oxidizing atmospheres) are much smaller than BZY and GDC. Because the Ba-deficient $Ba_3Y_4O_9$ main phase in the sample is considered to be dominant in the conductivity, it is a good ionic conductor at the intermediate temperatures. In the meanwhile, the crystallographic information of Ba-deficient $Ba_3Y_4O_9$ is needed to reveal the mechanism of the ionic conduction and the improvement of chemical

stability by the Zr substitution. Therefore we are now working on further investigation.

Acknowledgment

Reference

[1] B.C.H. Steele and A. Heinzel, *Nature*, **414**, 345 (2001).

[2] A. Dubois, S. Ricote, and R.J. Braun, *J. Power Sources*, **369**, 65 (2017).

[3] H. Yahiro, K. Eguchi, and H. Arai, *Solid State Ionics*, **36**, 71 (1989).

[4] T. Shimonosono, Y. Hirata, Y. Ehira, S. Sameshima, and T. Horita, *J. Ceram. Soc. Jpn.*, **112** (5), S616 (2004).

[5] T. Ishihara, H. Matsuda, and Y. Takita, *J. Am. Ceram. Soc.*, **116**, 3801 (1994).

[6] K. Huang, M. Feng, and J.B. Goodenough, *J. Am. Ceram. Soc.*, **79**, 1100 (1996).

[7] K.D. Kreuer, *Annu. Rev. Mater. Res.*, **33**, 333 (2003).

[8] D. Han and T. Uda, *J. Mater. Chem. A*, **6**, 18571 (2018).

[9] Y. Yamazaki, R. Hernandez-Sanchez, and S.M. Haile, *Chem. Mater.*, **21**, 2755 (2009).

[10] E. Fabbri, A. Depifanio, E. Dibartolomeo, S. Licoccia, and E. Traversa, *Solid State Ionics*, **179**, 558 (2008).

[11] D. Han, Y. Noda, T. Onishi, N. Hatada, M. Majima, and T. Uda, *Int. J. Hydrogen Energy*, **41**, 14897 (2016).

[12] H. Zhu, S. Ricote, C. Duan, R.P. O'Hayre, D.S. Tsvetkov, and R.J. Kee, *J. Electrochem. Soc.*, **165**,

F581 (2018).

[13] K. Katahira, Y. Kohchi, T. Shimura, and H. Iwahara, *Solid State Ionics*, **138**, 91 (2000).

[14] T. Onishi and T. Uda, *Electrochemistry*, **87**, 162 (2019).

[15] T. Nakamura, S. Mizunuma, Y. Kimura, Y. Mikami, K. Yamauchi, T. Kuroha, N. Taniguchi, Y. Tsuji, Y. Okuyama, and K. Amezawa, *J. Mater. Chem. A*, **6**, 15771 (2018).

[16] K. Ueno, N. Hatada, D. Han, K. Toyoura, and T. Uda, *J. Solid State Electrochem.*, **24**, 1523 (2020).

[17] M. Feng and J.B. Goodenough, *Solid State Ionics*, **68**, 269 (1994).

[18] J. Darriet and M.A. Subramanian, *J. Mater. Chem.*, **5**, 543 (1995).

[19] S. Fang, A. Takagaki, M. Watanabe, J.T. Song, and T. Ishihara, *Applied Catalysis A: General*, **602**, 117743 (2020).

[20] S. Fang, A. Takagaki, M. Watanabe, and T. Ishihara, *Catal. Sci. Technol.*, **10**, 2513 (2020).

[21] K. Goto, H. Matsumoto, and T. Ishihara, *Topics in Catalysis*, **52**, 1776 (2009).

[22] S. Devi, A. Khatkar, A. Hooda, V.B. Taxak, P. Boora, P. Dhankhar, and S.P. Khatkar, *J. Solid State Chem.*, **288**, 121333 (2020).

[23] A. Hooda, S.P. Khatkar, A. Khatkar, R.K. Malik, M. Kumar, S. Devi, and V.B. Taxak, *J. Luminescence*, **217**, 116806 (2020).

[24] J. Li, R. Pang, Z. Yu, L. Liu, H. Wu, H. Li, L. Jiang, S. Zhang, J. Feng, and C. Li, *J. Rare Earths*, **36**, 680 (2018).

[25] S. Liu, H. Ming, J. Cui, S. Liu, W. You, X. Ye, Y. Yang, H. Nie, and R. Wang, *J. Phys. Chem. C*, **122**, 16289 (2018).

[26] S. Liu, J. Cui, L. Liu, W. You, M.C. Parmar, Q. Zeng, R. Wang, and X. Ye, *J. Luminescence*, **213**, 174 (2019).

[27] S. Fop, K.S. McCombie, E.J. Wildman, J.M.S. Skakle, J.T.S. Irvine, P.A. Connor, C. Savaniu, C. Ritter, and A.C. Mclaughlin, *Nat. Mater.*, **19**, 752 (2020).

[28] T. Murakami, J.R. Hester, and M. Yashima, *J. Am. Chem. Soc.*, **142**, 11653 (2020).

[29] B. Szymanik, R.G. Buckley, H.J. Trodahl, and R.L. Davis, *Solid State Ionics*, **109**, 223 (1998).

[30] H. Kobayashi, K. Nakamura, T. Mori, H. Yamamura, and T. Mitamura, *Denki Kagaku Oyobi Kogyo Butsuri Kagaku*, **64**, 683 (1996).

[31] P. Babilo, T. Uda, and S.M. Haile, *J. Mater. Res.*, **22**, 1322 (2007).

[32] E.H.P. Cordfunke, A.S. Booij, R.J.M. Konings, R.R. Van Der Laan, V.M. Smit-Groen, and P. Van Vlaanderen, *Thermochimica Acta*, **273**, 1 (1996).

[33] K. Amezawa, Y. Uchimoto, and Y. Tomii, *Solid State Ionics*, **177**, 2407 (2006).

[34] A. Magrasó, C. Frontera, D. Marrero-López, and P. Núñez, *Dalton Transactions*, 10273 (2009).

[35] D. Han, K. Kato, and T. Uda, *Chemical Communications*, **53**, 12684 (2017).

Supplemental information

The microstructure of Zr-substituted Ba₃Y₄O₉

Fig. S1 shows the secondary electron images of cross-section and relative densities of the samples after the sintering. Dense pellets of the B3Y4-Z10 and B3Y4-Z20 samples were obtained whereas a pellet with pores was obtained in the B3Y4-Z0 sample. The grain sizes are several micrometers in the samples and the size of closed pores in the B3Y4-Z0 sample is 10-50 μm. When the Zr content increases, the boundaries between grains are observed clearly and the relative density becomes high. The morphology of the microstructure of the B3Y4-Z0 sample suggests the existence of the liquid phase.
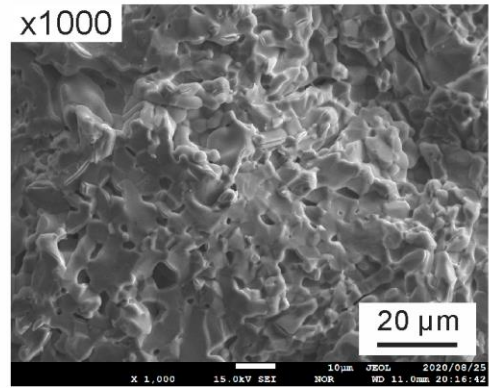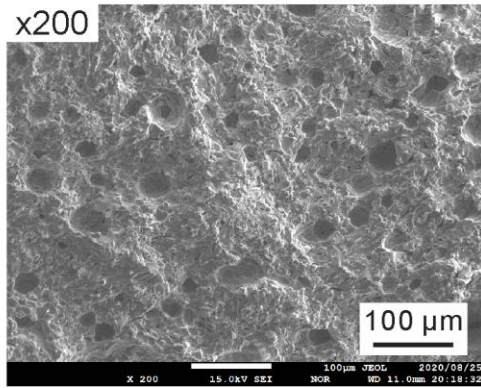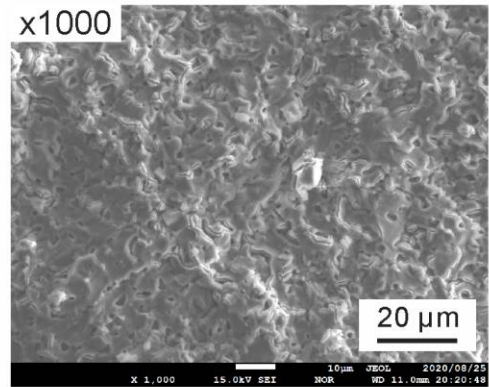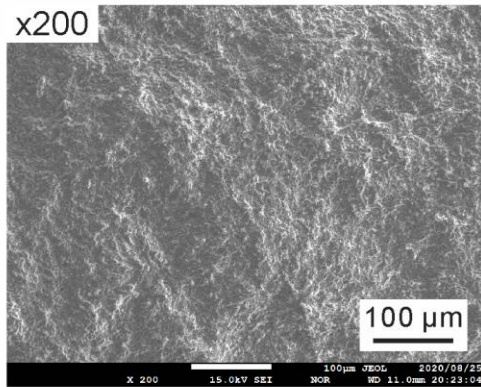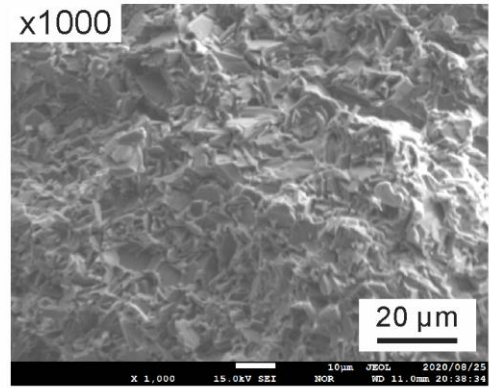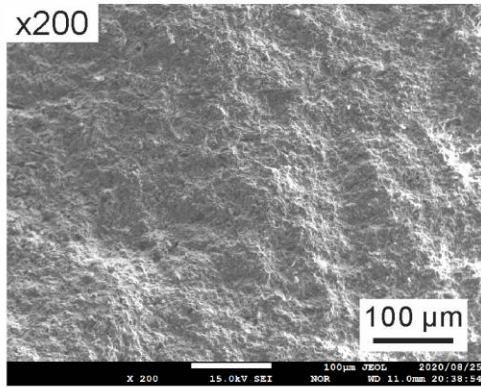
Fig. S5 The secondary electron images of the cross-section of (a) B3Y4-Z0, (b) B3Y4-Z10, and (c) B3Y4-Z20 pellets. All samples were sintered at 1600 °C for 24 hours in dry Ar-20 % O_2. The apparent density of the samples was measured by the Archimedes method and the relative density to the theoretical density of $Ba_3Y_4O_9$ was calculated.